J. Electroanal. Chem., 256 (1988) 291–307
Elsevier Sequoia S.A., Lausanne – Printed in The Netherlands

Digital simulations of cyclic voltammetry for the CE_q and CE_qC_2 mechanisms

Roger D. Moulton and Allen J. Bard *

Department of Chemistry, The University of Texas, Austin, TX 78712 (U.S.A.)

Stephen W. Feldberg

Department of Applied Science, Brookhaven National Laboratory, Upton, NY 11973 (U.S.A.)

(Received 26 February 1988; in revised form 22 June 1988)

ABSTRACT

The cyclic voltammetric behavior for two electrochemical reaction mechanisms, the CE_q (a quasi-reversible electron transfer following a preexisting chemical equilibrium) and CE_qC_{2i} (a CE_q reaction followed by an irreversible second-order reaction) were studied. To allow calculations at high homogeneous reaction rates, digital simulations with the heterogeneous equivalent (HE) approach were employed. Zone diagrams for both cases are presented, and the characteristic behavior in limiting regions is discussed. Working curves for analysis of the behavior in intermediate regions are also presented.

INTRODUCTION

In this paper, we describe the cyclic voltammetric (CV) behavior for two electrochemical reaction mechanisms: the CE_q case, (a reversible chemical reaction preceding a quasi-reversible electron transfer, eqns. 1 and 2); and the CE_qC_2 case (a CE_q mechanism in which a second-order reaction occurs following electron transfer, eqns. 1–3). The CE mechanism has been treated for cases where the electron transfer (eqn. 2) is nernstian [1–3] or totally irreversible [3]. On the other hand, no effort has been made to evaluate the CV behavior of the CE mechanism in the general case; i.e., when the heterogeneous electron-transfer kinetics may be only moderately slow. In the course of simulating the CE_qC_2 reaction scheme it was also

* To whom correspondence should be addressed.

0022-0728/88/$03.50

possible to treat the CE case where heterogeneous electron transfer kinetics are sluggish.

$$Y \underset{k_{-1}}{\overset{k_1}{\rightleftarrows}} A \qquad K_1 = k_1/k_{-1} \tag{1}$$

$$A + e^- \underset{k_b}{\overset{k_f}{\rightleftarrows}} B \qquad E^{\circ\prime} \tag{2}$$

$$2\,B \underset{k_{-2}}{\overset{k_2}{\rightleftarrows}} X \qquad K_2 = k_2/k_{-2} \tag{3}$$

Equations (1)–(3) describe the CE_q and CE_qC_{2i} mechanisms in terms of an electrochemical reduction. However, we were motivated to consider these mechanisms during our studies [4] of the oxidation of cyclopentadiene (CpH) in liquid ammonia. In that example, the CpH is in equilibrium with the deprotonated form, Cp^-. Oxidation of Cp^- to the radical is followed by dimerization to the species Cp_2. For the analysis of oxidation waves, an analogous treatment of the CV wave as for reductions can be carried out; effects such as shifts in potential with scan rate, K_1, etc. are the same value in each case (reversed in direction), and the cathodic transfer coefficient α is replaced by the anodic transfer coefficient $(1 - \alpha)$.

Because the dimerization is fast and irreversible for the CpH study, we limit our discussion here of the CE_qC_2 behavior to cases where λ_2 $(= k_2 c^\circ RT/nFv) \gg 1$ and and $k_{-2} = 0$ (CE_qC_{2i}). To our knowledge, there are no previous reports in the literature of the CE_qC_{2i} case (eqns. 1–3), either experimental or theoretical. The voltammetric behavior of these electrode reactions will be discussed, based on computer modeling of the reaction mechanisms.

Digital simulation of electrochemical mechanisms has been carried out for a variety of different mechanisms and experiments [5,6]. The goal of those studies was to determine the diagnostic criteria most helpful in the quantitative evaluation of the reaction mechanism. The analysis of electrode mechanisms often utilizes finite difference digital simulation modeling [7]. This method becomes inefficient when fast homogeneous reaction kinetics effect a reaction layer that becomes much smaller than the diffusion layer. Several methods have been employed to save time in the calculations. Notable among the several approaches are the use of expanding space [8,9] and time [10] grids, implicit [11] and "hopscotch" modeling [12–15] and orthogonal collocation [16,17]. All of these techniques are helpful in reducing the computation time; however, in the limit, as the coupled reactions become very fast, the calculations require unreasonable amounts of time. Another technique, dubbed the heterogeneous equivalent (HE) [18], can be used when the reaction layer is much smaller than the diffusion layer. Efficient computation is effected by coupling an analytical solution for the reaction layer phenomena with direct simulation of bulk diffusion. The rate constants for the cyclopentadiene system appear to meet the conditions for the use of the HE.

THEORY

The HE defines a semi-analytical solution for the current function, in which the flux equation for the electron transfer is replaced by an expression which combines the concentrations of the bulk species and the heterogeneous and homogeneous rate constants. In this way, the direct simulation of the concentrations of transient species in the reaction layer is obviated. Heterogeneous and reaction layer phenomena may all be considered to occur at the plane of the electrode surface. Therefore, the HE method is most precise for thin reaction layers. The HE was combined with an explicit finite difference program with an expanding (exponential) space grid. HE simulations were carried out for the CE_q case (eqns. 1 and 2), in which electron transfer is quasi-reversible. The effect of changes in the heterogeneous and homogeneous rate constants were explored, and experimental methods of evaluating these assessed. The results are compared to the previously reported [1–3] behavior of the CE_R and CE_i mechanisms. We also derive an HE expression for a CE_q process in which the product undergoes an irreversible second-order following reaction (e.g. dimerization) to an electroinactive product, and analyze the CV behavior of this mechanism.

CE_q case

As mentioned above, the heterogeneous equivalent was used in conjunction with a finite difference program with an expanding exponential grid [19] to simulate the CV response of the mechanism. To maximize the efficiency of the calculations, digital simulations of electrochemical experiments are usually performed by using dimensionless parameters: diffusion, fluxes, and rate constant. The HE for the CE_q case has been derived previously [18] and an explicit expression for the flux of species Y in the reaction layer $(f_Y)_\mu$ was obtained. The dimensionless equation for the flux (dimensionless parameters are indicated by an asterisk) may be obtained by replacing the variables in the previously described flux equation with their dimensionless analogues, which are defined in the Glossary. This leads to eqn. (4) (comprising only dimensionless simulation parameters) which is used to calculate the flux (the dimensionless current Z is calculated from $Z = ((f_Y^*)_\mu/c^\circ)((D_Y Fvn/RT)^{1/2})$ in a finite-difference program with the previously described [7] format. The original derivation of this expression requires several assumptions concerning the homogeneous rate constants, which are listed in eqns. (5) and (6).

$$(f_Y^*)_\mu = (Y_1^* - B_1^*/\theta K_1)/(1/k_{HE3}^* + \gamma/D_Y^* + 1/K_1 k_f^* + \gamma/\theta K_1 D_B^*) \quad (4)$$

$$K_1 \ll 1 \quad (5)$$

$$\lambda_1 = (k_1 + k_{-1})RT/nFv > 10 \quad (6)$$

$$k_{HE3}^* = (K_1 k_f^* D_A^*)^{1/2} \quad (7)$$

The fluxes calculated with eqn. (4) agree [18] with direct simulation or analytical solutions (when available). The restriction in eqn. (5) can be removed, if an alternative expression [20] is used to calculate the HE of a more general case, i.e., for any value of K_1. The term γ is defined as the distance from the electrode where

the average concentration of Y in the first volume element is presumed to be located. For a linear grid, $\gamma = 0.5$ (i.e., the average concentration is in the center of the box). The mechanisms based on eqns. (1)–(3) were simulated with an exponential grid using $\beta = 0.20$ (β is the exponential factor for the grid [9]: $\Delta x_i = \Delta x \exp(\beta(i-1))$. The γ-value can be obtained from $\gamma = (\exp(\beta/2) - 1)/\exp(\beta) - 1)$, which for $\beta = 0.2$ gives $\gamma = 0.475$. When Y and A are in fast equilibrium (i.e. the HE is an appropriate solution for the flux), $k_{HE3} \rightarrow \infty$, and eqn. (4) reduces to

$$(f_Y^*)_\mu = (k_f' Y_1^* - k_b^* B_1^*)/(1 + k_1'^* \gamma/D_Y^* + k_b^* \gamma/D_B^*) \quad (8)$$

where $k_f'^* = k_f^* K_1$. This expression is identical to that derived for the quasi-reversible case, in which Y is reduced directly at the electrode to B. The preceding equilibrium has the effect of slowing the electron transfer process in the forward direction without affecting the backward rate. Since the forward reaction is more sluggish, the reduction occurs at a more negative potential than $E^{\circ\prime}$. The observed reduction potential ($E^{\circ\prime\prime}$) has been shown [1–3] to be related to K_1 by $E^{\circ\prime\prime} = E^{\circ\prime} + (RT/nF) \ln K_1$. Consider now a new heterogeneous rate equation, in which $E^{\circ\prime}$ in the Butler–Volmer equation is substituted with $E^{\circ\prime\prime} - (RT/nF) \ln K_1$:

$$k_f = k^\circ K_1 \exp[-\alpha nF/RT\{E - E^{\circ\prime\prime} + (RT/nF) \ln K_1\}] \quad (9)$$

or

$$k_f = k_{HE} \exp[-\alpha nF/RT(E - E^{\circ\prime\prime})] \quad (10)$$

$$k_{HE} = k^\circ K_1^{(1-\alpha)} \quad (11)$$

This new preexponential term is the equivalent of the standard heterogeneous rate constant. A similar calculation of k_b gives the same preexponential term, which confirms that k_{HE} is the HE rate constant for the "couple" Y/B.

In summary, the effect of the preceding equilibrium is to shift the redox couple to a more negative potential (for a reduction, positive for an oxidation) because the unfavorable equilibrium decreases the forward heterogeneous rate constant. The apparent heterogeneous rate constant for the Y/B couple decreases because the heterogeneous kinetics are affected by the shift in redox potential.

CE_qC_{2i} case

From the previously described [18] steady-state solutions to the CE_q and E_qC_2 cases, the following flux equations have been obtained. The HE flux expression can be derived by solving for $(f_Y)_\mu$ as a function of the chemical and simulation parameters (each of the terms are defined in the Glossary):

$$(f_A)_0 = k_f A_0 - k_b B_0 \quad (12)$$

$$(f_Y)_\mu = D_Y(Y_1 - Y_\mu)/\gamma \Delta x \quad (13)$$

$$(f_Y)_\mu = (f_A)_0 \quad (14)$$

$$(f_B)_0 = -(f_A)_0 \quad (15)$$

$$(f_A)_0 = D_A(K_1 Y_\mu - A_0)(k_{-1}/D_A)^{1/2} \quad (16)$$

$$(f_B)_0 = (4D_B/3)^{1/2}\left[\left(K_2^{-1} X_\mu\right)^{1/2} - B_0\right]\left[k_2\left\{2\left(K_2^{-1} X_\mu\right)^{1/2} + B_0\right\}\right]^{1/2} \quad (17)$$

In the limit as $k_{-2} \rightarrow 0$ (and therefore $K_2 \rightarrow \infty$), eqn. (17) simplifies to

$$(f_B)_0 = -(4/3)^{1/2} D_B^{1/2} k_2^{1/2} B_0^{3/2} \tag{18}$$

Equations (16) and (17) are derived from the steady-state analytical solutions to the differential equations which describe the electrochemical sequence. The following assumption was made for eqn. (18) to be valid (eqns. 5 and 6 also apply):

$$\lambda_2 = k_2 c^\circ RT/nFv > 100 \tag{19}$$

Starting with eqn. (12), we can obtain

$$B_0 = (k_f A_0 - (f_A)_0)/k_b \tag{20}$$

With eqns. (14) and (16), we have

$$A_0 = K_1 Y_\mu - (f_Y)_\mu/(D_A k_{-1})^{1/2} \tag{21}$$

Rearranging eqn. (13) gives

$$Y_\mu = Y_1 - (f_Y)_\mu \gamma \Delta x/D_Y \tag{22}$$

Combining eqns. (21) and (22),

$$A_0 = K_1(Y_1 - (f_Y)_\mu \gamma \Delta x/D_Y) - (f_Y)_\mu/(D_A k_{-1})^{1/2} \tag{23}$$

and defining $\theta = k_f/k_b$, eqns. (20) and (23) give

$$B_0 = \theta K_1(Y_1 - (f_Y)_\mu \gamma \Delta x/D_Y) - \theta(f_Y)_\mu/(D_A k_{-1})^{1/2} - (f_Y)_\mu/k_b \tag{24}$$

Substituting in eqn. (18), we arrive at

$$[c - a(f_Y)_\mu]^3 = b^2 (f_Y)_\mu^2 \tag{25}$$

where

$$a = \theta K_1 \gamma \Delta x/D_Y + \theta/(D_A k_{-1})^{1/2} + 1/k_b \tag{26}$$

$$b^2 = 3/(4 D_B k_2) \tag{27}$$

$$c = \theta K_1 Y_1 \tag{28}$$

The solution of $(f_Y)_\mu$ in eqn. (25) represents the HE expression for the flux in the CE_qC_{2i} case. As mentioned before, we require that the simulations be carried out using dimensionless parameters, and so it is necessary to convert a, b, and c to their dimensionless counterparts, so that the expression yields a dimensionless flux:

$$[c^* - a^*(f_Y^*)_\mu]^3 = b^{*2}(f_Y^*)_\mu^2 \tag{29}$$

where

$$a\Delta x/\Delta t = a^* = \theta K_1 \gamma/D_Y^* + \theta/(D_A^* k_{-1}^*)^{1/2} + 1/k_b^* \tag{30}$$

$$(b\Delta t/\Delta x)^2 c^\circ = b^{*2} = 3/(4 D_B^* k_2^*) \tag{31}$$

$$c/c^\circ = c^* = \theta K_1 Y_1^* \tag{32}$$

Equation (29) can be solved numerically for $(f_Y^*)_\mu$ by using, for example, the binary method [19]. The flux is used to calculate new concentrations of Y and B in the first box (at the electrode surface). Calculation of the dimensionless current and diffusion into the bulk solution is carried out later in the iteration loop.

RESULTS

CE_q behavior

As in other CV treatments of reaction schemes [1–3,5,6,21], it is convenient to represent behavior in terms of dimensionless parameters (these dimensionless parameters are combinations of real world variables, and are to be distinguished from the dimensionless parameters used to optimize the calculations). For the CE_q case these are [1,2] $\lambda_1 K_1^2$ $(\lambda_1 = (k_{-1} + k_1)RT/nFv)$ and [3] $\Lambda K_1^{(1-\alpha)}$ $(\Lambda = (k^\circ(D_A/D_B)^{\alpha/2})/(D_A nvF/RT)^{1/2})$. Typical CV waves for different values of λ_1 and Λ are shown in Fig. 1a–d. Pure diffusional currents (i.e. constant $i_p/v^{1/2}$; Figs.

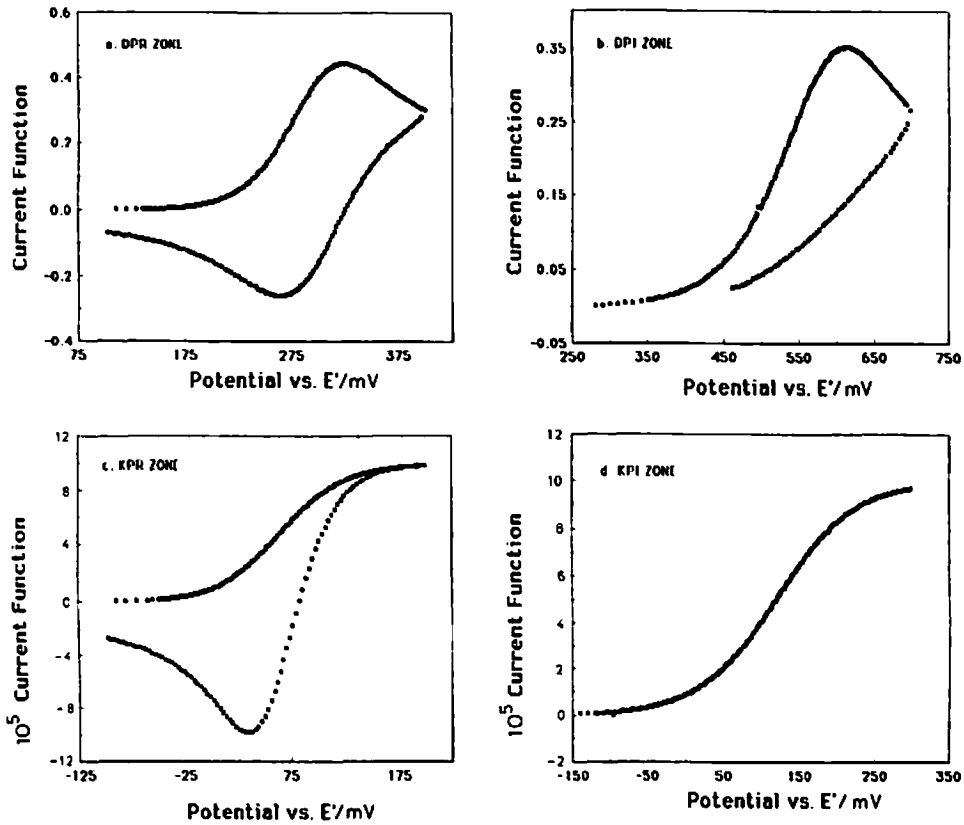

Fig. 1. Cyclic voltammograms for CE_q case. (a) $K_1 = 10^{-5}$; $\lambda_1 = 10^{20}$; $\Lambda = 10^{20}$; (b) $K_1 = 10^{-5}$; $\lambda_1 = 10^{20}$; $\Lambda = 1$; (c) $K_1 = 10^{-5}$; $\lambda_1 = 10^{-3}$; $\Lambda = 10^{20}$; (d) $K_1 = 10^{-5}$; $\lambda_1 = 10^{-3}$; $\Lambda = 1$.

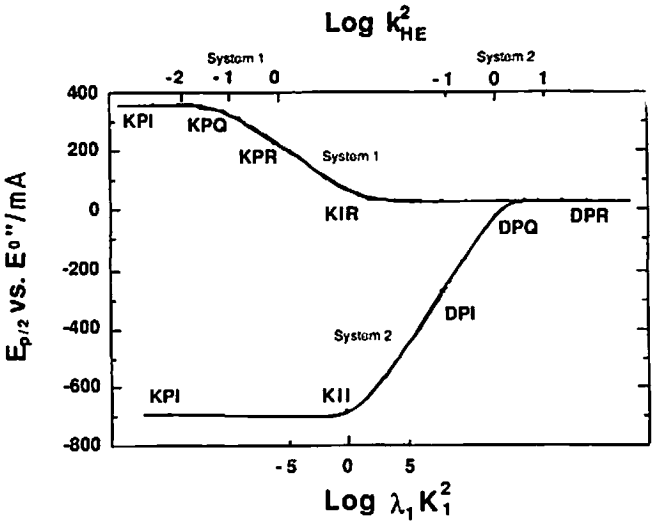

Fig. 2. Working curves for scan rate dependance of $E_{p/2}$ for the CE_q mechanism. In system 1, $\lambda_1 K_1^2 \gg k^2_{HE}$, and k^2_{HE}(upper abscissa) can be determined in the KPQ zone. In the KIR zone, $\lambda_1 K_1^2$(lower abscissa) can be obtained. In system 2, $\lambda_1 K_1^2 \ll \Lambda K_1^{(1-\alpha)}$, and values of $\lambda_1 K_1^2$ and k^2_{HE} can be obtained in the KII and DPQ zones, respectively.

1a and b) are obtained for the CE case when $\lambda_1 K_1^2$ is large and pure kinetic currents (i_p independent of v; Figs. 1c and d) result when $\lambda_1 K_1^2$ is small. Similarly, large values of k_{HE} lead to nernstian behavior; smaller values lead to quasi-reversibility and irreversibility. In the following discussion, purely diffusional currents will be referred to as DP currents, whereas purely kinetic currents will referred to as KP. A situation in which the kinetic contribution is significant but not dominant will be referred to as intermediate kinetics, KI. Similarly, the letter following the KP, KI, or DP designation refers to the reversibility (R), quasi-reversibility (Q), and irreversibility (I) in the heterogeneous electron transfer.

The contribution of heterogeneous kinetics to the waveform for diffusional waves is usually determined by ΔE_p ($= E_{pc} - E_{pa}$) measurements, which for the CE_q case is directly related to k_{HE}. An alternative approach, based on the shift of the half-peak potential $E_{p/2}$ with scan rate, provides information about both the heterogeneous and homogeneous rates. In Fig. 2, the half-peak potential $E_{p/2}$ is plotted against scan rate for two hypothetical chemical systems (system 1: $\lambda_1 K_1^2 \ll \Lambda K_1^{(1-\alpha)}$, and system 2: $\lambda_1 K_1^2 \gg \Lambda K_1^{(1-\alpha)}$). At very slow scan rates, $\lambda_1 K_1^2$ and $\Lambda K_2^{(1-\alpha)}$ are large for both systems, and $E_{p/2}$ is independent of scan rate in this region. If the homogeneous rate becomes slow (at faster scan rates, system 1), the half-peak potential shifts in a positive direction, reaching a slope of $29/n$ mV at 25 C. On the other hand, if the heterogeneous kinetics become sluggish (system 2), then $E_{p/2}$ moves in a negative direction with a slope of $-30/\alpha n$ mV. At very fast scan rates, $\lambda_1 K_1^2$ and $\Lambda K_1^{(1-\alpha)}$ are both small. In this case, $E_{p/2}$ again becomes

independent of scan rate, because the positive shift brought on by the homogeneous kinetics is balanced by the negative shift due to the heterogeneous kinetics. The value of $E_{p/2}$ (in mV) within each limiting region may be obtained from eqns. (33)–(36), which were derived from the data in Fig. 2:
In the DPR zone,

$$E_{p/2} = E^{\circ\prime\prime} + 1.09RT/nF \tag{33}$$

In the KPR zone.

$$E_{p/2} = E^{\circ\prime\prime} - (0.351RT/nF) - (RT/2nF)\ \ln(v/k_{-1}) \tag{34}$$

In the KPI zone,

$$E_{p/2} = E^{\circ\prime\prime} - (RT/\alpha nF)\left[4.93 - \ln\ k_{HE} + \ln(\alpha nF/RT)^{1/2}\right] + (RT/2\alpha nF)\ \ln(k_{-1}) \tag{35}$$

In the DPI zone,

$$E_{p/2} = E^{\circ\prime\prime} - (RT/\alpha nF)\left[2.85 - \ln\ k_{HE} + \ln(\alpha nFv/RT)^{1/2}\right] \tag{36}$$

The $E_{p/2}$ plot shown in Fig. 2 can be used as a working curve and compared with experimental $E_{p/2}$ vs. scan rate data to obtain values of $\lambda_1 K_1^2$ and $\Lambda K_1^{(1-\alpha)}$. For example, if a given point on the $E_{p/2}$ plot can be shown to correspond to a value of k_{HE} or $\lambda_1 K_1^2$ on the working curve, from the definition of these parameters a value of $k_1 K_1^2$ or $k^\circ K_1^{(1-\alpha)}$ can be calculated. If $\lambda_1 K_1^2 \approx \Lambda K_1^{(1-\alpha)}$, then the $\Delta E_{p/2}/\Delta$ log v behavior is more complicated. The dependence of the behavior of the system on K_1 requires an independent estimate of its value before values of k_1 and k° can be obtained.

The waveshape of a quasi-reversible electron transfer reaction has been shown previously [2] to be a useful indicator of the electrode kinetics. In the case of the CE_q mechanism, the waveshape is especially useful, since, as will be shown in the following discussion, the homogeneous rate constants can also be estimated from it. The waveform in the case of diffusional waves is often examined by $|E_p - E_{p/2}|$ measurements [3,22]. However, this requires an accurate measurement of the peak potential, which is difficult, due to the smoothness of the curve near the maximum. It is because of this difficulty, for example, that $\Delta E/\Delta$ log v measurements are often made by using $E_{p/2}$ (rather than E_p). This problem is compounded in the analysis of kinetic currents (which show no CV peak). Therefore, we reintroduce the $|E_{3/4} - E_{1/4}|$ criterion, borrowed from the analysis of polarographic waves, as a means of describing the waveshape. In Fig. 3, the variation of $|E_{3/4} - E_{1/4}|$ with $\Lambda K_1^{(1-\alpha)}$ is plotted for the purely diffusional and kinetic cases. Purely kinetic CVs display waves with essentially the same waveshape as the corresponding polarographic waves, so the heterogeneous constants (such as α, $E_{1/2}$, $\Lambda K_1^{(1-\alpha)}$, etc.) may also be determined by the Tomes [23,24] and Randles [25] method.

It has been shown previously [1,2] for the CE_R case that the CV peak current is more sensitive to the preceding homogeneous kinetics than is the peak potential

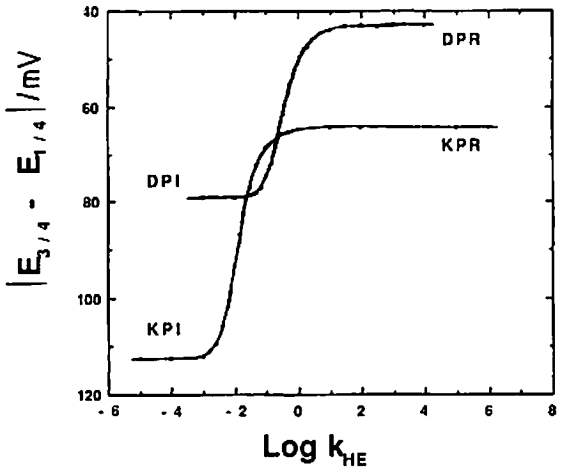

Fig. 3. Values of $|E_{3/4} - E_{1/4}|$ in DPQ and KPQ zones for the CE_q mechanism. $T = 298$ K.

value. Thus, the transition zone between purely diffusional and purely kinetic behavior is wider using this indicator. In Fig. 4a, the dimensionless peak current for the CV waves is plotted against changes in $\log \lambda_1 K_1^2$ for different values of $\Lambda K_1^{(1-\alpha)}$. In the limit $\lambda_1 K_1^2 \ll 1$, the peak current becomes constant, and does not change with scan rate (Fig. 4b).

It is helpful to condense the behavior in Figs. 2–4 into a zone diagram, so that the voltammetric behavior can be predicted on the basis on the values of $\Lambda K_1^{(1-\alpha)}$, and $\lambda_1 K_1^2$ (Fig. 5). The horizontal boundaries in Fig. 5 (relating to changes in $\lambda_1 K_1^2$) are based on peak current measurements (assumed to be accurate to $\pm 5\%$).

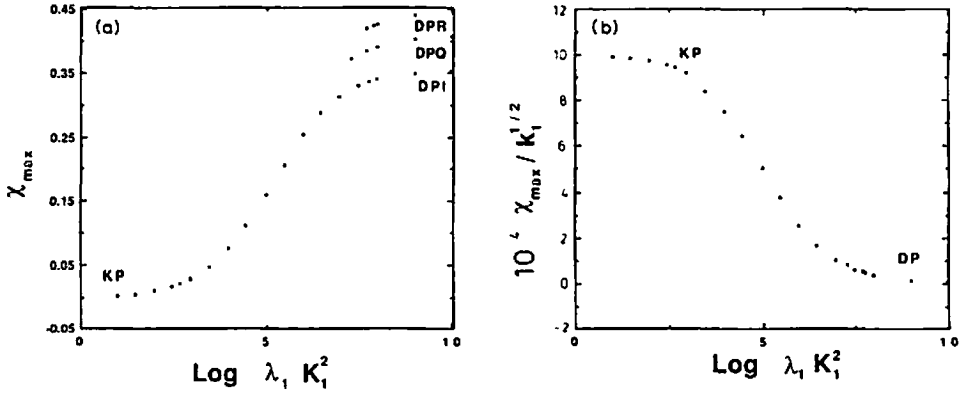

Fig. 4. (a) Variation of the dimensionless current maximum χ_{max} with λ_1 for CE_q case. In DPR curve, $\Lambda K_1^{(1-\alpha)} = 10^{10}$; in DPQ curve, $\Lambda K_1^{(1-\alpha)} = 1$; in DPI curve, $\Lambda K_1^{(1-\alpha)} = 10^{-3}$. (b) Change in current function adjusted to constant $k_1^{1/2}$ vs. λ_1.

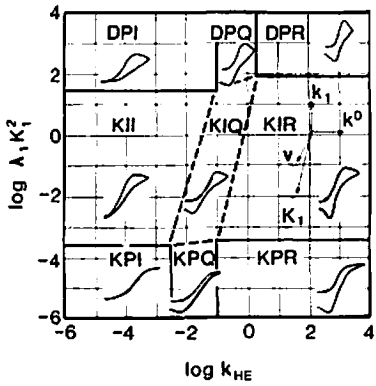

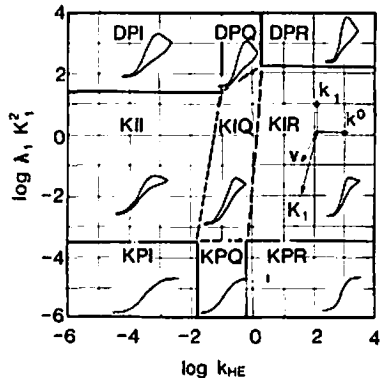

Fig. 5. Zone diagram for the CE_q mechanism.

Fig. 6. Zone diagram for the CE_qC_{2i} mechanism. The simulations that were used to derive the boundary lines assumed $\lambda_2 = 10^{10}$.

The vertical boundaries (based on changes in k_{HE}) are based on $|E_{3/4} - E_{1/4}|$, assuming an accuracy of ± 5 mV. The locations of the boundaries between the zones in Fig. 5 are listed in Table 1. In Fig. 5, typical CV traces in each zone (analogous to Figs. 1a–d) are illustrated, and the effect of a 10-fold increase in scan rate (v), K_1, k_1, and k° is shown by directions and magnitudes of the arrows.

Figure 5 shows that 9 zones of possible behavior exist for the CE case. Four of the regions (DPR, DPI, KPR, KPI) are limiting cases where values of $\Lambda K_1^{(1-\alpha)}$ and $\lambda_1 K_1^2$ are not available from the CV experiment. In the intermediate zones, a comparison of the working curves shown in Figs. 2–4 with experimental data provides values for the rates of each reaction. The most difficult case to treat is the KIQ zone, since the waveform (based on $|E_{3/4} - E_{1/4}|$) is affected by both the heterogeneous and homogeneous kinetics. Since no single current function describes this case, working curves of the voltammetric behavior are unavailable.

TABLE 1

Values of boundary lines in Figs. 5 and 6 for CE_q and CE_qC_{2i} mechanisms. For the CE_qC_{2i} case, λ_2 was taken at 10^{10}. $T = 298$ K

Boundary	CE_q case	CE_qC_{2i} case
DPR/DPQ	$k_{HE} = 10^{0.3}$	$k_{HE}(\lambda_2)^{1/6} = 10^{0.3}$
DPQ/DPI	$k_{HE} = 10^{-1}$	$k_{HE}(\lambda_2)^{1/6} = 10^{-1}$
KPR/KPQ	$k_{HE} = 10^{-1.1}$	$k_{HE} = 10^{-0.2}$
KPQ/KPI	$k_{HE} = 10^{-2.5}$	$k_{HE} = 10^{-1.8}$
DPR/KIR	$\lambda_1 K_1^2 = 10^{1.9}$	$\lambda_1 K_1^2 = 10^{2.2}$
KIR/KPR	$\lambda_1 K_1^2 = 10^{-3.5}$	$\lambda_1 K_1^2 = 10^{-3.5}$
DPI/KII	$\lambda_1 K_1^2 = 10^{1.4}$	$\lambda_1 K_1^2 = 10^{1.4}$
KII/KPI	$\lambda_1 K_1^2 = 10^{-3.5}$	$\lambda_1 K_1^2 = 10^{-3.5}$

CE_qC_{2i} case

The behavior of the CE_qC_{2i} case (in the limit of large values of the dimensionless second-order rate constant $\lambda_2 = k_2 c^\circ RT/\nu nF$) is qualitatively similar to the CE_q case described above, and a zone diagram analogous to Fig. 5 can be derived (Fig. 6). In the following discussion, the same terminology (DPI, KIQ, etc.) will be used to describe each of the individual zones. The most immediately obvious difference between the two mechanisms is the lack of an anodic peak on the return scan in the CE_qC_{2i} case, due to the rapid disappearance of the reduced species B. Representative CVs in the limiting regions are shown in Fig. 7a–d.

As has been shown in previous treatments of the E_qC_{2i} case, when the electron transfer is totally irreversible, the fate of the reduced species is irrelevant to the shape of the voltammetric wave. Thus in the limit as $k_{HE} \ll 1$ the behavior of the CE_q and CE_qC_{2i} mechanisms is identical. On the other hand, if the electron transfer is faster, the following reaction causes the reduction potential to shift positive of its

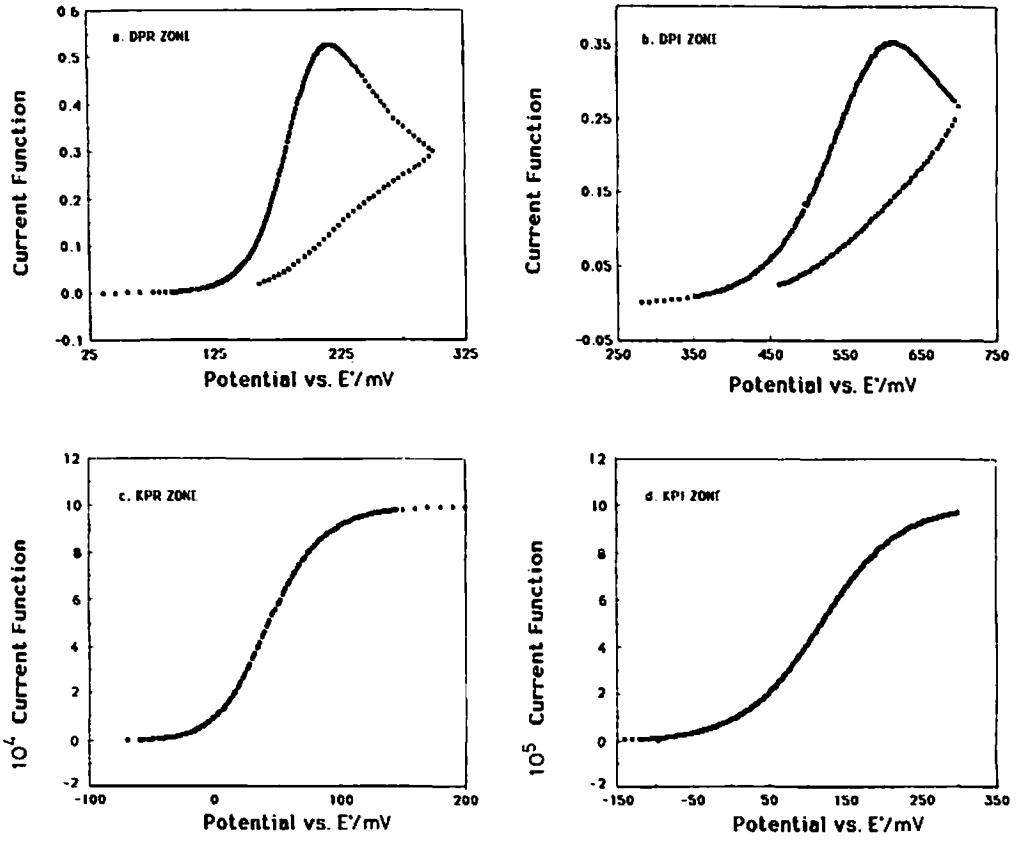

Fig. 7. Typical CV traces for CE_qC_{2i} mechanism. (a) $\Lambda = 10^{20}$; $\lambda_1 = 10^{19}$; $\lambda_2 = 10^5$; $K_1 = 10^{-5}$; (b) $\Lambda = 1$; $\lambda_1 = 10^{19}$; $\lambda_2 = 10^{20}$; $K_1 = 10^{-5}$; (c) $\Lambda = 10^{20}$; $\lambda_1 = 0.001$; $\lambda_2 = 10^5$; $K_1 = 10^{-5}$; (d) $\Lambda = 1$; $\lambda_1 = 0.001$; $\lambda_2 = 10^{20}$; $K_1 = 10^{-5}$.

TABLE 2

Selected diagnostic criteria in limiting regions (Figs. 5 and 6) for CE_q and CE_qC_{2i} mechanisms

Criteria	Zone			
	DPR	DPI	KPR	KPI
CE_q case				
$\Delta E_{p/2}/\Delta \log v$	0	$-1.15RT/\alpha nF$	$1.15RT/nF$	0
i_p	constant $i_p/v^{1/2}$		constant i_p	
$E_{3/4} - E_{1/4}$	$1.63RT/nF$	$1.52RT/\alpha nF$	$2.49RT/nF$	$2.18RT/\alpha nF$
ΔE_p	$2.3RT/nF$	$> 2.3RT/nF$	–	–
CE_qC_{2i} case				
$\Delta E_{p/2}/\Delta \log v$	$-0.76RT/nF$	$-1.15RT/\alpha nF$	0	0
i_p	same as CE_q case			
$E_{3/4} - E_{1/4}$	$1.09RT/nF$	$1.52RT/\alpha nF$	$1.87RT/nF$	$2.18RT/\alpha nF$

reversible value. This shift has the effect of decreasing the electron transfer kinetics by a factor of $\lambda_2^{1/6}$ for the E_qC_{2i} case [26,27]. Similarly, in the DPR and DPQ zones of Fig. 6, the values of $|E_{3/4} - E_{1/4}|$ behave according to:

$$k_{HE} = \Lambda K_1^{(1-\alpha)} \lambda_2^{1/6} \tag{37}$$

In Fig. 6 arrows indicate the effect of a decade change in the parameters as previously mentioned above for Fig. 5. The effect of changes in scan rate are not

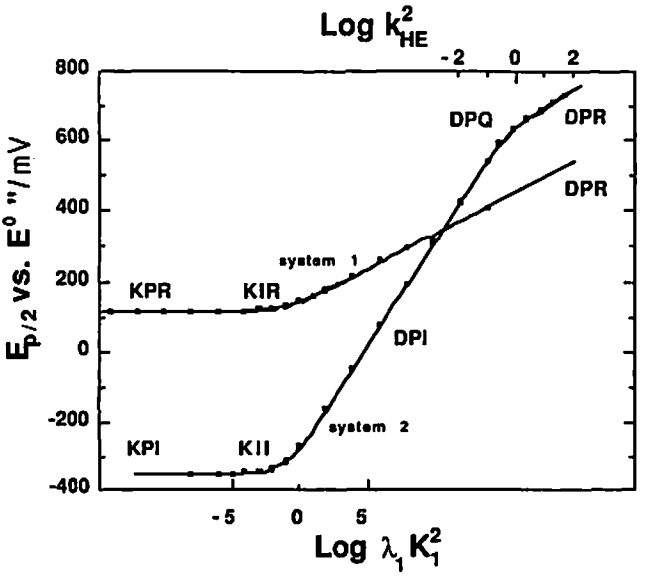

Fig. 8. Working curves for scan rate dependence of $E_{p/2}$ vs. scan rate for the CE_qC_{2i} mechanism. In system 1, $\lambda_1 K_1^2 \gg k^2_{HE}$. In the KIR zone, $\lambda_1 K_1^2$(lower abscissa) can be obtained by comparison with scan rate data. In system 2: $\lambda_1 K_1^2 \ll k^2_{HE}$, and values of $\lambda_1 K_1^2$ and k^2_{HE}(upper abscissa) can be obtained in the KII and DPQ zones, respectively.

TABLE 3

Values of current function in KPR zone for CE_qC_{2i} mechanism

Potential/mV	Current function [b]	Potential/mV	Current function [b]
−112.900	1.929×10^{-6}	1.200	5.141×10^{-4}
−102.900	3.452×10^{-6}	3.200	5.371×10^{-4}
−92.900	6.166×10^{-6}	5.200	5.598×10^{-4}
−84.900	9.786×10^{-6}	7.200	5.821×10^{-4}
−82.900	1.098×10^{-5}	9.200	6.038×10^{-4}
−80.900	1.231×10^{-5}	11.200	6.250×10^{-4}
−78.900	1.381×10^{-5}	13.200	6.455×10^{-4}
−76.900	1.548×10^{-5}	15.200	6.654×10^{-4}
−74.900	1.735×10^{-5}	17.200	6.845×10^{-4}
−72.900	1.944×10^{-5}	19.200	7.030×10^{-4}
−70.900	2.176×10^{-5}	21.200	7.206×10^{-4}
−68.900	2.437×10^{-5}	23.200	7.375×10^{-4}
−66.900	2.727×10^{-5}	25.200	7.537×10^{-4}
−64.900	3.049×10^{-5}	27.200	7.690×10^{-4}
−62.900	3.408×10^{-5}	29.200	7.836×10^{-4}
−60.900	3.807×10^{-5}	31.200	7.975×10^{-4}
−58.900	4.249×10^{-5}	33.200	8.106×10^{-4}
−56.900	4.739×10^{-5}	35.200	8.230×10^{-4}
−54.900	5.281×10^{-5}	37.200	8.347×10^{-4}
−52.900	5.879×10^{-5}	39.200	8.457×10^{-4}
−50.900	6.539×10^{-5}	41.200	8.561×10^{-4}
−48.900	7.264×10^{-5}	43.200	8.659×10^{-4}
−46.900	8.059×10^{-5}	45.200	8.750×10^{-4}
−44.900	8.929×10^{-5}	47.200	8.835×10^{-4}
−42.900	9.879×10^{-5}	49.200	8.917×10^{-4}
−40.800	1.096×10^{-4}	51.200	8.992×10^{-4}
−38.800	1.209×10^{-4}	53.200	9.063×10^{-4}
−36.800	1.331×10^{-4}	55.200	9.129×10^{-4}
−34.800	1.462×10^{-4}	57.200	9.190×10^{-4}
−32.800	1.603×10^{-4}	61.200	9.301×10^{-4}
−30.800	1.753×10^{-4}	65.200	9.397×10^{-4}
−28.800	1.913×10^{-4}	69.200	9.481×10^{-4}
−26.800	2.084×10^{-4}	73.200	9.553×10^{-4}
−24.800	2.262×10^{-4}	77.200	9.616×10^{-4}
−22.800	2.451×10^{-4}	81.200	9.670×10^{-4}
−20.800	2.647×10^{-4}	85.200	9.716×10^{-4}
−18.800	2.852×10^{-4}	89.200	9.756×10^{-4}
−16.800	3.064×10^{-4}	93.200	9.790×10^{-4}
−14.800	3.282×10^{-4}	97.200	9.820×10^{-4}
−12.800	3.506×10^{-4}	102.200	9.851×10^{-4}
−10.800	3.734×10^{-4}	107.200	9.877×10^{-4}
−8.800	3.966×10^{-4}	117.200	9.915×10^{-4}
−6.800	4.201×10^{-4}	127.200	9.942×10^{-4}
−4.800	4.436×10^{-4}	137.200	9.960×10^{-4}
−2.800	4.672×10^{-4}	147.200	9.972×10^{-4}
−0.800	4.907×10^{-4}	157.100	9.980×10^{-4}
0.000	5.000×10^{-4}		

[a] Potential axis is vs. $E_{p/2}$.

[b] Current function is normalized to constant $k_1^{1/2}$.

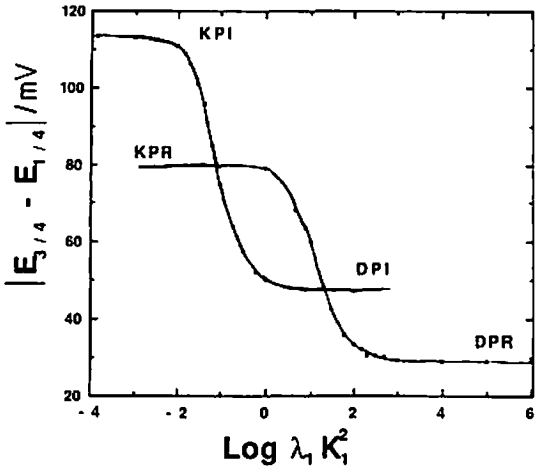

Fig. 9. Variation of $|E_{3/4} - E_{1/4}|$ in KPQ and DPQ zones for the CE_qC_{2i} case.

constant over the entire diagram. If $\Lambda K_2^{(1-\alpha)}$ is small, then the arrow should have a slope of 2, as in Fig. 5. But if eqn. (37) holds (DPR and DPQ zones), then the slope is 13/6. The slope of the arrow in the other zones is between these values. Since the variation is small, the arrow in the diagram was drawn with a slope of 2, as in Fig. 5.

The voltammetric characteristics of the CE_qC_{2i} case are summarized in Table 2. In the DPR zone (in the limit as $\Lambda K_1^{(1-\alpha)} \to \infty$) the peak is significantly sharper than for the CE_q case in the DPR zone. The waveshape in this zone (sometimes referred to [26] as "super-reversible" because of the small value of $E_p - E_{p/2}$) is the same as for the E_RC_{2i} case [22], with fast heterogeneous and homogeneous kinetics. In the KPR zone, no peak is observed on either the negative or positive scans (in

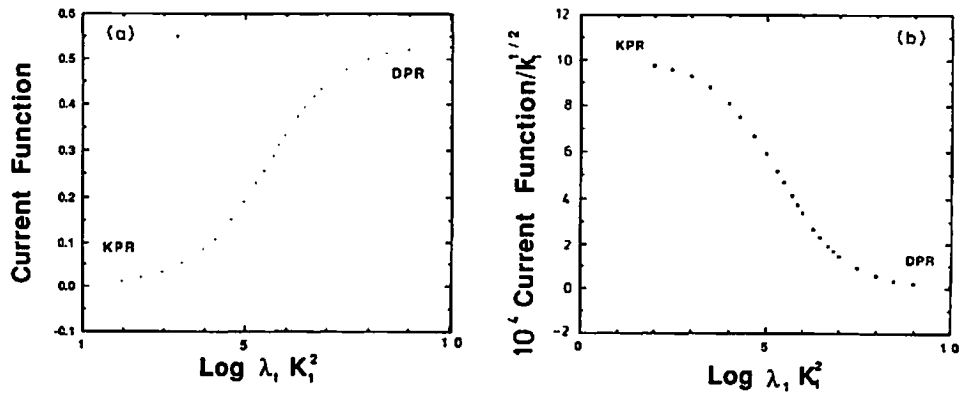

Fig. 10. Variation of current function maximum vs. λ_1 across KPR and DPR zones for CE_qC_{2i} case (current normalized to constant $K_1^{1/2}$) vs. λ_1. (b) Variation of current function maximum vs. λ_1 for CE_qC_{2i} mechanism.

contrast to Fig. 1c). As the current function for this wave has not been described previously, its values are tabulated in Table 3.

In summary, the behavior of the CE_q and CE_qC_{2i} mechanisms are similar and can be distinguished only when the heterogeneous kinetics are at least moderately fast. $|E_{3/4} - E_{1/4}|$ and the maximum value of the current function are good diagnostic criteria for the limiting cases for both mechanisms. To determine the rates of the individual reactions in the intermediate zones (KPQ, DPQ, KIR, and KII), working curves of $E_{p/2}$ (Figs. 2 and 8), $|E_{3/4} - E_{1/4}|$ (Figs. 3 and 9) and peak current (Figs. 4 and 10) can be used in the way described earlier for the CE_q case.

CONCLUSIONS

The HE flux expressions (eqns. 4 and 19) represents a useful method of digital simulation of the CE_q and CE_qC_{2i} mechanisms. With this method, the dependence of CV peak current and waveshape on changes in the scan rate, equilibrium constant, and the heterogeneous and homogeneous rates was determined. The HE represents a useful approach which saves computational time during the simulation of electrochemical problems, so that the current–potential behavior can be obtained.

If the CE_q (or the CE_qC_{2i}) case is suspected for a system (e.g. CpH in ammonia), the location in the zone diagram (Figs. 5 and 6) may be found from the voltammetric characteristics of the wave, available in Figs. 2–4 and Table 2. Generally, peak current and $|E_{3/4} - E_{1/4}|$ values can yield estimates of the rate constants for both mechanisms. Information about the kinetics may also be obtained from peak location in the intermediate regions with peak potential vs. scan rate plots. In the accompanyzing paper [4], we illustrate this by analyzing the CE_2C_{2i} mechanism for the oxidation of cyclopentadiene.

ACKNOWLEDGEMENTS

This work was supported by the National Science Foundation grant No. CHE 8402135. J.W.F. gratefully acknowledges the Division of Chemical Science, United States Department of Energy, Washington, DC, under contract No. DE-AC02-76CH00016.

GLOSSARY

Parameter	Unit	Definition (eqn. parameter first appeared)
k_1, k_{-1}	s^{-1}	homogeneous first-order rate constants for eqn. 1 (1)
k_1^*, k_{-1}^*	–	dimensionless first-order rate constants ($= k_1 \Delta t$) (7)
k_2, k_{-2}	$mol^{-1}\ s^{-1}$	homogeneous second-order rate constants for eqn. 3 (3)

k_2^*, k_{-2}^*	–	dimensionless second-order rate constants for eqn. 3 ($= k_2\ \Delta t c^\circ$) (31)
K_1, K_2	mol^x	equilibrium constant (1)
k_f, k_b	cm s^{-1}	forward and backward heterogeneous rate constants for eqn. 2 (2)
k_b^*, k_f^*	–	dimensionless heterogeneous rates ($= k_b\ \Delta x/\Delta t$)
k°	cm s^{-1}	standard heterogeneous rate constant (9)
k_{HE}	–	$\Lambda K_1^{(1-\alpha)}$, dimensionless heterogeneous rate constant for CE_q case (10)
k_{HE3}^*	–	$(K_1 k_1^* D_A^*)^{1/2}$ (4)
$(f_M)_0$	$\text{mol cm}^{-1}\ \text{s}^{-2}$	flux of the Mth species at $x = 0$ (12)
$(f_M)_\mu$	$\text{mol cm}^{-2}\ \text{s}^{-1}$	flux of the Mth species at $x = \mu$ (13)
$(f_M^*)_{0\text{ or }\mu}$	–	dimensionless flux at $x = 0$ or μ ($= (f_M)_x\ \Delta t/\Delta x c^\circ$) (4)
μ	cm	reaction layer thickness (4)
A_N, $B_N \ldots$	mol cm^{-3}	concentrations of species A, B... in Nth volume element (12)
A_N^*, $B_N^* \ldots$	–	dimensionless concentrations (A_N/c°) of species A, B... in Nth element (4)
D_M	$\text{cm}^2\ \text{s}^{-1}$	actual diffusion coefficient of Mth species (13)
D_M^*	–	dimensionless diffusion coefficient of Mth species: $D_M\ \Delta t/\Delta x^2$ (4)
θ	–	$k_f/k_b = \exp(\alpha n F(E - E^{\circ\prime})/RT)$ (4)
$E^{\circ\prime}$	V	standard reduction potential of couple A/B (2)
$E^{\circ\prime\prime}$	V	$E^{\circ\prime} - RT/nF\ \ln K_1/(1 + K_1)$ (9)
c°	mol cm^{-3}	bulk concentration of species initially present (19)
α	–	transfer coefficient (9)
n	–	number of electrons (6)
Λ	–	dimensionless heterogeneous rate constant (37)
λ_1, λ_2	–	normalized homogeneous rate constants for eqns. (1) and (3) (6)
$E_{1/4}$, $E_{p/2}$, $E_{3/4}$	V	1/4-peak, half-peak and 3/4-peak potentials (33)
γ	–	point of average concentration in the first box/size of the first box (4)
β	–	exponential function of the grid [9]
Δx	cm	size of the first box (13)
Δx_i	cm	size of ith box ($= \Delta x \exp\{\beta(i-1)\}$)
Δt	s	time between each iteration (see above)

REFERENCES

1 J.M. Savéant and E. Vianello, Electrochim. Acta, 8 (1963) 905.
2 J.M. Savéant and E. Vianello, Electrochim. Acta, 12 (1967) 629.

3 R.S. Nicholson and I. Shain, Anal. Chem., 36 (1964) 706.
4 R.D. Moulton, R. Farid and A.J. Bard, J. Electroanal. Chem., 256 (1988) 309.
5 M.K. Hanafey, R.L. Scott, T.H. Ridgway and C.N. Reilley, Anal. Chem., 50 (1978) 116.
6 C.P. Andrieux and J.M. Savéant in C.F. Bernasconi (Ed.), Investigations of Rates and Mechanisms of Reactions, Vol. 6, 4/E, Part 2, Wiley, New York, 1986, p. 352.
7 S.W. Feldberg in A.J. Bard (Ed.), Electroanalytical Chemistry, Vol. 3, Marcel Dekker, New York, 1969, p. 199.
8 T. Joslin and D. Pletcher, J. Electroanal. Chem., 49 (1974) 171.
9 S.W. Feldberg, J. Electroanal. Chem., 127 (1981) 1 and references therein.
10 R. Seeber and S. Stefani, Anal. Chem., 53 (1981) 1011.
11 J. Heinze, J. Electroanal. Chem., 124 (1981) 73.
12 D. Shoup and A. Szabo, J. Electroanal. Chem., 160 (1984) 1.
13 D. Shoup and A. Szabo, J. Electroanal. Chem., 140 (1982) 237.
14 D. Shoup and A. Szabo, J. Electroanal. Chem., 160 (1984) 19.
15 D. Shoup and A. Szabo, J. Electroanal. Chem., 160 (1984) 27.
16 B. Speiser, S. Pons and A. Rieker, Electrochim. Acta, 27 (1982) 1171.
17 S. Pons in A.J. Bard (Ed.), Electroanalytical Chemistry, Vol. 13, Marcel Dekker, New York, 1984, p. 115.
18 I. Ruzic and S. Feldberg, J. Electroanal. Chem., 50 (1974) 153.
19 S.W. Feldberg in J.S. Mattson, H.B. Mark and H.C. MacDonald, Jr. (Eds.), Computers in Chemistry and Instrumentation, Vol. 2, Marcel Dekker, New York, 1972, p. 202.
20 I. Ruzic, J. Electroanal. Chem., 144 (1983) 433.
21 A.J. Bard and L.R. Faulkner, Electrochemical Methods, Wiley, New York, 1980, p. 219.
22 M.L. Olmstead, R.G. Hamilton and R.S. Nicholson, Anal. Chem., 41 (1969) 260.
23 J. Tomes, Collect. Czech. Chem. Commun., 9 (1937) 12.
24 L. Meites and Y. Israel, J. Electroanal. Chem., 8 (1964) 99.
25 J.E.B. Randles, Can. J. Chem., 37 (1959) 238.
26 D.H. Evans, J. Phys. Chem., 76 (1972) 1160.
27 L. Nadjo and J.M. Savéant, J. Electroanal. Chem., 48 (1973) 113.